AGU PUBLICATIONS

Geophysical Research Letters

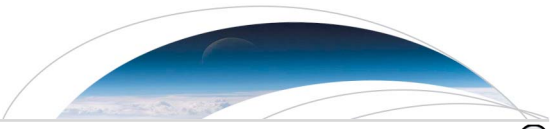

RESEARCH LETTER

10.1002/2014GL062081

Key Points:
- Sea ice model uncertainty estimates increase spread for subseasonal predictions
- Seasonal prediction estimates not affected by sea ice model uncertainties

Supporting Information:
- Readme
- Figure S1
- Figure S2

Correspondence to:
S. Juricke,
Stephan.Juricke@awi.de

Citation:
Juricke, S., H. F. Goessling, and T. Jung (2014), Potential sea ice predictability and the role of stochastic sea ice strength perturbations, *Geophys. Res. Lett.*, *41*, 8396–8403, doi:10.1002/2014GL062081.

Received 2 OCT 2014
Accepted 16 NOV 2014
Accepted article online 18 NOV 2014
Published online 9 DEC 2014

Potential sea ice predictability and the role of stochastic sea ice strength perturbations

Stephan Juricke[1,2], Helge F. Goessling[1], and Thomas Jung[1]

[1] Alfred Wegener Institute, Helmholtz Centre for Polar and Marine Research, Bremerhaven, Germany, [2] Atmospheric, Oceanic and Planetary Physics, University of Oxford, Oxford, UK

Abstract Ensemble experiments with a climate model are carried out in order to explore how incorporating a stochastic ice strength parameterization to account for model uncertainty affects estimates of potential sea ice predictability on time scales from days to seasons. The impact of this new parameterization depends strongly on the spatial scale, lead time and the hemisphere being considered: Whereas the representation of model uncertainty increases the ensemble spread of Arctic sea ice thickness predictions generated by atmospheric initial perturbations up to about 4 weeks into the forecast, rather small changes are found for longer lead times as well as integrated quantities such as total sea ice area. The regions where initial condition uncertainty generates spread in sea ice thickness on subseasonal time scales (primarily along the ice edge) differ from that of the stochastic sea ice strength parameterization (along the coast lines and in the interior of the Arctic). For the Antarctic the influence of the stochastic sea ice strength parameterization is much weaker due to the predominance of thinner first year ice. These results suggest that sea ice data assimilation and prediction on subseasonal time scales could benefit from taking model uncertainty into account, especially in the Arctic.

1. Introduction

The opportunities and risks associated with polar climate change have increased the demand for sea ice predictions substantially. This has increased development efforts of sea ice prediction systems [e.g., *Chevallier et al.*, 2014; *Sigmond et al.*, 2013]. However, akin to atmospheric predictions [e.g., *Lorenz*, 1963], sea ice predictions are limited due to the chaotic nature of the climate system. Recently, there have been a number of studies exploring the upper limits of predictability—or potential predictability—in the Arctic [e.g., *Koenigk and Mikolajewicz*, 2009; *Blanchard-Wrigglesworth et al.*, 2011; *Holland et al.*, 2011; *Tietsche et al.*, 2014] and the Antarctic [*Holland et al.*, 2013] on seasonal to interannual time scales.

While these studies differ in the details of the approaches, models, and diagnostics used, they are based on the assumption that perfect knowledge of the initial state would result in a perfect prediction. More specifically, limits of potential predictability using the so called "perfect model" assumption are obtained by applying small perturbations to the initial state in order to generate ensembles. The growth in ensemble spread can then be compared to the level of interannual model variability, and potential predictability is said to be lost once the ensemble spread is equal to the level of interannual variability.

At the same time there has been an increasing number of publications dealing with ways to represent model uncertainty (for an introduction see *Palmer* [2012]). While in a deterministic model formulation the mean impact of the subgrid scale processes on the resolved scale dynamics is simulated, stochastic methods can be used to include higher-order moments into the formulation of subgrid scale parameterizations. Instead of always using the best estimate for the mean impact of subgrid scale processes, deviations from the best estimate that occur when averaging over finite-sized grid cells are conveyed to the resolved dynamics. Including stochastic aspects in the model formulation may not only improve the general representation of the subgrid scale processes and the related uncertainties; in addition, it may also improve the simulation of the large-scale flow [*Palmer*, 2012]. Uncertainties in the parameterizations of subgrid scale processes have previously been represented by the use of stochastic parameterizations [e.g., *Lin and Neelin*, 2002; *Bright and Mullen*, 2002; *Plant and Craig*, 2008; *Li et al.*, 2008; *Lott et al.*, 2012]. In weather forecasts, incorporation of uncertainty estimates for the subgrid scales has lead to an improved model performance [e.g., *Buizza et al.*, 1999; *Shutts*, 2005; *Jung et al.*, 2005; *Weisheimer et al.*, 2011]. These efforts, however, have concentrated on stochastic parameterizations for atmospheric models. Furthermore, the impact of incorporating

stochastic aspects in climate models has recently been analyzed in view of changes to the simulated mean climate [e.g., *Williams*, 2012; *Juricke et al.*, 2013; *Juricke and Jung*, 2014; *Brankart*, 2013].

In this study, potential predictability of sea ice is estimated in a coupled climate model for which the "perfect model" assumption is relaxed by employing stochastic sea ice strength perturbations to represent uncertainties in the formulation of the sea ice rheology. More specifically, the ensemble spread generated solely by atmospheric initial perturbations is compared to the spread that is generated when model uncertainty is accounted for by including the stochastic sea ice strength parameterization by *Juricke et al.* [2013] and *Juricke and Jung* [2014]. In addition, ensembles comprising both, atmospheric initial perturbations and stochastic sea ice dynamics, are analyzed. The objective is to assess whether the upper limits of subseasonal to seasonal predictability of sea ice as obtained in so called "perfect model" studies are sensitive to the incorporation of the stochastic perturbations simulating uncertainties in the ice strength parameterization.

2. Experimental Setup

2.1. Model

The ensemble experiments of this study were carried out with the global coupled model European Centre/HAMburg, version 6 - Finite Element Sea ice Ocean Model (ECHAM6-FESOM) [*Sidorenko et al.*, 2014]. The atmospheric component ECHAM6 [*Stevens et al.*, 2013] of the Max-Planck-Institute for Meteorology in Hamburg is a spectral model employing a horizontal resolution of about 1.85° with 47 vertical levels up to 0.01 hPa (T63L47). By using the Ocean Atmosphere Sea Ice Soil, version 3 - Model Coupling Toolkit (OASIS3-MCT) [*Valcke*, 2013] coupler, ECHAM6 is coupled to FESOM [*Danilov et al.*, 2004; *Wang et al.*, 2008; *Timmermann et al.*, 2009; *Sidorenko et al.*, 2011; *Wang et al.*, 2013], which has been developed at the Alfred Wegener Institute, Helmholtz Centre for Polar and Marine Research. The effective resolution of the unstructured triangular ocean surface grid ranges from $\sim$ 150 km in the open ocean to $\sim$ 25 km near the coasts, in the Arctic, and along the equatorial belt. In the vertical the ocean model uses a tetrahedral grid with 46 unevenly spaced z levels. The time steps used for FESOM and ECHAM6 are 30 and 10 min, respectively, with coupling taking place every 6 h. The mean sea ice thickness distribution simulated under present-day (1990) forcing is in good agreement with observational estimates (see Figures S1 and S2 in the supporting information), suggesting that the model is well suited for the purpose of this study. Further details regarding the model formulation and its performance in simulating the mean climate are described in the study by *Sidorenko et al.* [2014].

2.2. Simulations

The ensemble size for each of the following configurations and start dates is 10 ensemble members. Each ensemble configuration has 15 start years, initialized both on the first of January and first of July at 00 UTC. The length of each forecast is 1 year. Consecutive start years are separated by 10 year intervals to ensure independent initial states. The initial conditions for the ensemble forecasts are provided by a multicentennial ECHAM6-FESOM simulation—after about 440 years into the simulation—under constant present-day (1990) forcing [*Sidorenko et al.*, 2014]. A 100 year period is used for the initial perturbations and consists of the first 100 years covered by the ensemble start dates. Sea ice concentration and thickness fields are available at a 6-hourly (averaged) resolution.

Four different sets of ensembles have been generated. In the first ensemble configuration (INI) integrations were initialized with atmospheric initial perturbations for the three-dimensional wind and temperature and two-dimensional surface pressure using the random field method introduced by *Magnusson et al.* [2009]. The method creates perturbations "in approximate flow balance" [*Magnusson et al.*, 2009] by adding downscaled differences between two randomly chosen atmospheric states of the same time of the year (here from a 100 year control integration). The difference fields are scaled with the factor 0.1, giving on average perturbations of a similar magnitude to the one described by *Magnusson et al.* [2009]. In contrast to other more qualitative perturbation methods applied in "perfect model" type studies, such as lagged atmospheric state initialization (e.g., *Koenigk and Mikolajewicz* [2009], typically stronger than 10% random field perturbations) and SST white noise perturbations (e.g., *Tietsche et al.* [2014], typically weaker than 10% random field perturbations), the realistic atmospheric initial perturbation strength provided by the random field method allows meaningful quantitative comparisons when it comes to assessing the effect of stochastic perturbations also at short lead times. Other than the described random field perturbations all initial fields for each of the members of the same ensemble are identical. This ensemble configuration serves as a reference for estimating potential sea ice predictability without accounting for model uncertainty.

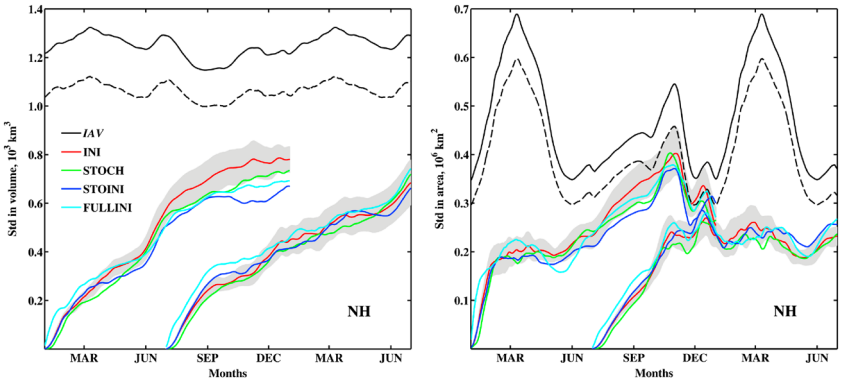

Figure 1. Ensemble spread (mean standard deviation of individual forecast ensembles) for Arctic sea ice (left) volume (10^3 km^3) and (right) area (10^6 km^2) for the four different ensemble configurations: atmospheric random field initial perturbations (INI, red), stochastic sea ice strength perturbations (STOCH, green), atmospheric random field initial perturbations combined with stochastic sea ice strength perturbations (STOINI, blue), and initialization with random atmospheric states (FULLINI, cyan). Twelve months forecasts were started at 00 UTC on 1 January and 1 July. Also shown is the annual cycle of the interannual standard deviation from the control simulation (*IAV*, black). The 6-hourly data have been smoothed by a 7 day running mean filter. The gray shaded area is the 95% confidence interval for INI; and the dashed line marks the lower limit of the 95% confidence interval for *IAV*. Confidence intervals were obtained by bootstrapping with 1000 samples.

In the second ensemble experiment (STOCH) atmospheric and oceanic initial conditions were left unperturbed. Instead, ensemble spread was generated using the stochastic sea ice strength parameterization described by *Juricke and Jung* [2014]. This parameterization implements symmetric, Gaussian-like perturbations to the ice strength parameter P^* of the elastic-viscous-plastic sea ice rheology. The parameter P^* is not well constrained and cannot be measured directly, leading to large related uncertainties. Under the same sea ice conditions larger (smaller) values of P^* reduce (increase) convergent sea ice drift, which is why P^* is commonly used as a tuning parameter for the simulated sea ice distribution. The stochastic ice strength parameterization adds symmetric perturbations to the previously constant parameter P^*. The stochastic perturbations are correlated in time by a first-order Markov process and in space by a predefined correlation matrix [*Juricke and Jung*, 2014]. They are transformed into a limited and physically realistic range and applied to every ice covered ocean grid node during the course of the entire integration. The method therefore simulates uncertainties, including spatial and temporal coherence, in the choice of the internal ice strength and thus in the resistance of the ice to plastic deformation under convergent motion. Due to the highly nonlinear formulation of the sea ice rheology and its important role in the formation of thick ice under convergence, incorporating a stochastic component in the parameterization of the sea ice rheology is expected to lead to rapid generation of ensemble spread in areas of convergent sea ice drift with high concentrations of thick sea ice.

In the third ensemble configuration (STOINI), both the initial perturbations used in INI and the stochastic sea ice strength parameterization used in STOCH were employed. It therefore combines estimates of atmospheric initial condition uncertainty with estimates of model uncertainty in the simulation of the sea ice dynamics.

Finally, in the fourth ensemble experiment (FULLINI) atmospheric initial states including the land surface were chosen randomly (for the same calendar day) from the 100 year control integration also used for the perturbations in INI. This configuration allows to estimate the potential predictability of sea ice associated with the memory inherent to the sea ice and ocean components under the "perfect model" assumption. It reflects a maximum level of uncertainty for the atmospheric initial states.

3. Results

3.1. Arctic

The evolution of spread for ensemble predictions of integrated Arctic sea ice quantities throughout the forecast is shown in Figure 1 for the four different experiments. The ensemble spread of Arctic sea ice volume and area stays below the level of interannual variability throughout the 12 months forecast period,

highlighting that Arctic sea ice area and especially volume are potentially predictable at least 12 months ahead. This result is consistent with previous studies [e.g., *Tietsche et al.*, 2014].

Significant differences between the different ensemble configurations concerning ensemble spread of Arctic sea ice volume and area emerge during the first days and weeks of the forecasts, that is, during a period of relatively strong perturbation growth. Figure 1 suggests that the spread grows most rapidly for FULLINI followed by STOINI and INI, which show a similar behavior, at least for this particular metric. The smallest perturbation growth is found for STOCH. Notice, that although the differences between the experiments appear small during the first weeks of the forecast they are highly significant given the relatively narrow confidence intervals (shown for INI in Figure 1; confidence intervals for the other ensemble configurations are of similar magnitude).

After about 1 month into the forecast the growth of the spread of Arctic sea ice volume and area of the different ensemble experiments is comparable, if sampling uncertainty is taken into account (Figure 1). Notice in this context that confidence intervals for the ensemble spread broaden rapidly around 3–4 weeks into the forecast. Significant differences in sea ice volume spread are evident between STOINI and INI for winter start dates and long lead times. The somewhat counterintuitive result that the spread for long lead times is lower when model uncertainty is represented might have to do with changes in the mean sea ice thickness distribution resulting from the stochastic perturbations (see *Juricke and Jung* [2014] for a detailed discussion). However, given that FULLINI also shows reduced volume spread, whereas STOCH hardly does, suggests that the differences for longer lead time are due to sampling uncertainty.

Our results suggest that previous estimates of potential seasonal sea ice area and volume predictability remain largely unchanged if uncertainty in the sea ice dynamics of the model is accounted for by employing a stochastic sea ice strength parameterization. Furthermore, details on how atmospheric perturbations are generated in this study (namely, random field perturbations and randomly chosen atmospheric states of the same calendar day) play a secondary role in estimates of potential sea ice area and volume predictability on monthly to seasonal time scales. During the first weeks of the forecasts, however, FULLINI shows significantly more spread than the other three ensemble experiments, implying that considerable predictability for integrated sea ice quantities on subseasonal time scales originates from the atmospheric initial conditions.

In order to shed more light on the differences between the four experiments during the early stages of the forecast a more in-depth analysis has been carried out. The average ensemble spread of sea ice thickness during winter and summer for INI 5 days into the forecasts is shown in Figure 2 together with the corresponding interannual sea ice thickness variability (first and second rows). The ensemble spread is more than 1 order of magnitude smaller than the interannual variability, highlighting the importance of sea ice initialization for relatively short-term sea ice predictions. The largest ensemble spread for INI is found close to the ice edge, where atmospheric perturbations can have a large impact due to the presence of strong sea ice thickness and concentration gradients; comparably small values are found in the interior of the Arctic where sea ice thickness is relatively homogeneous and concentrations are high.

In Figure 2 (third row) the spread in sea ice thickness generated by the initial atmospheric perturbations is compared to the spread obtained from stochastic sea ice strength perturbations after 5 days. Evidently, the stochastic sea ice scheme generates significantly more spread during boreal winter in the region of large sea ice thickness north of Greenland and the Canadian Arctic Archipelago (CAA), that is, in a region where continuously thick and relatively immobile sea ice prevents atmospheric perturbations from having a sizable impact. Additional spread with stochastic sea ice perturbations is also found in the interior of the Arctic, both during boreal summer and winter. Therefore, our results show that the stochastic ice strength perturbations in STOCH significantly increase sea ice thickness spread primarily in the internal ice pack during the first few days of the forecast. In these regions the internal forces of the sea ice are the main opposing forces to atmospheric stresses in the simulation of the sea ice dynamics and therefore largely determine sea ice velocities. However, atmospheric perturbations produce sea ice spread rapidly, which tends to propagate from the ice edge toward the central ice pack. About 1 (July) to 3 (January) weeks into the forecast atmospherically generated spread in INI tends to surpass the spread generated by the stochastic sea ice parameterization in STOCH almost everywhere (not shown). This is especially true for the summer start dates, as during winter the sea ice thickness variability generated by internal sea ice dynamics is of considerable importance when compared with the impact of atmospheric forcing.

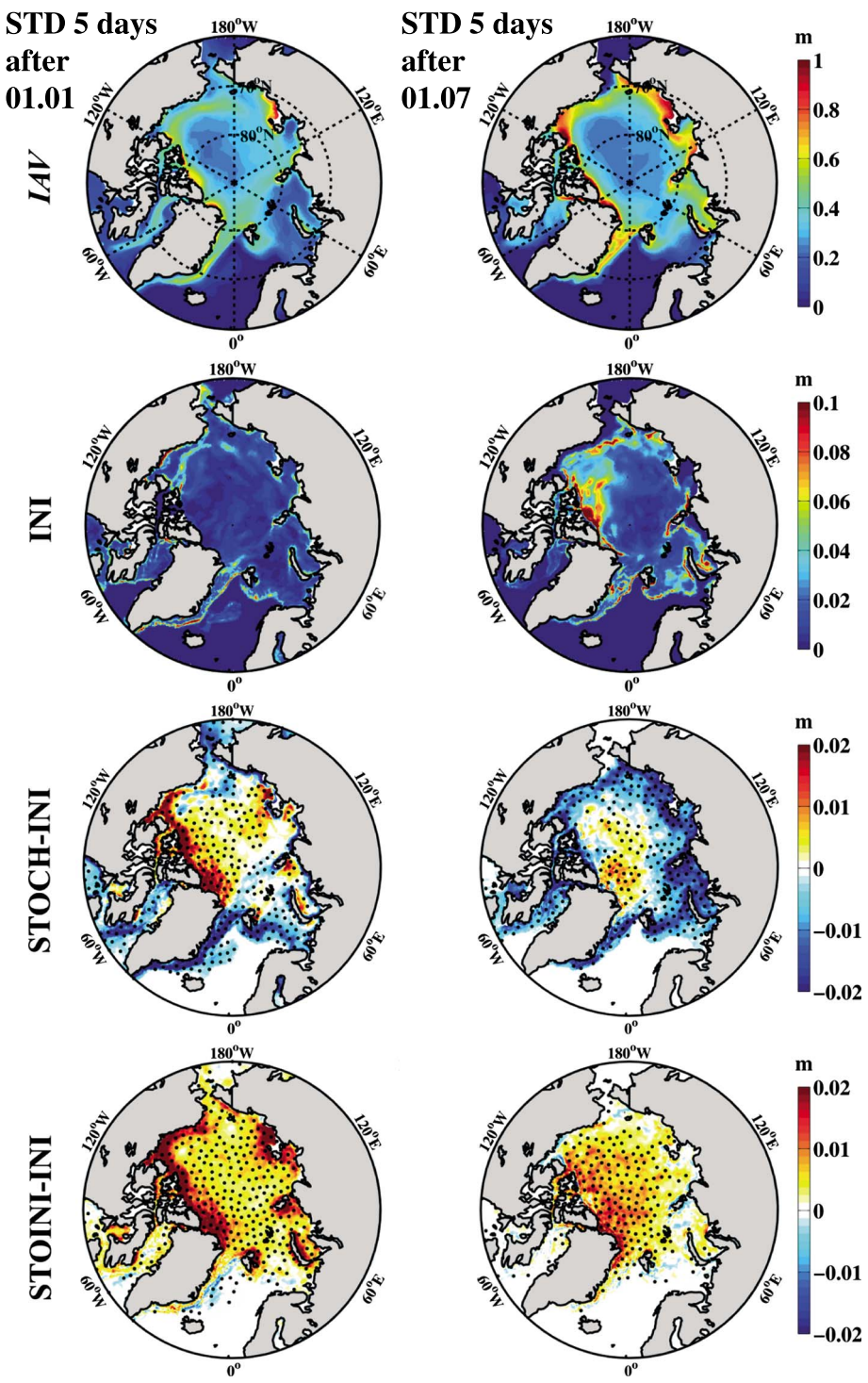

Figure 2. Mean standard deviation of sea ice thickness forecasts (meters) 5 days after initialization at 00 UTC on (left) 1 January and (right) 1 July. (first row) Interannual sea ice thickness standard deviation (*IAV*) for the control integration. (second row) Mean ensemble spread for INI. (third row) Difference in mean ensemble spread between STOCH and INI. (fourth row) Difference in mean ensemble spread between STOINI and INI. Stippled areas indicate differences statistically significant at the 5% level, using a two-tailed *F* test. Note the different contour intervals.

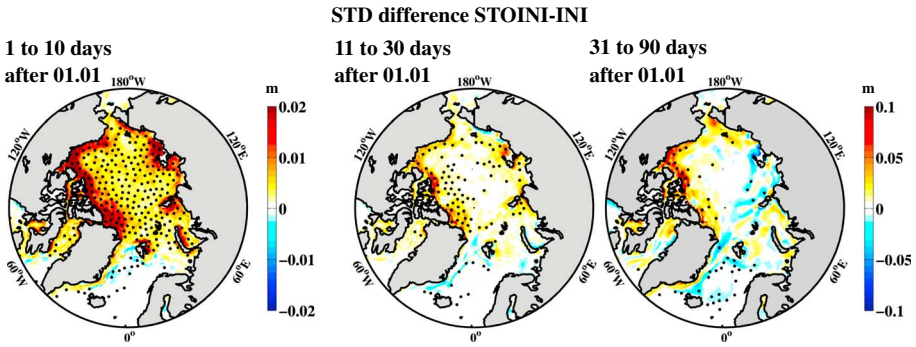

Figure 3. As in Figure 2 but for the difference between STOINI and INI, averaged for days (left) 1 to 10, (middle) 11 to 30, and (right) 31 to 90 after the initialization at 00 UTC on 1 January. Note the different contour intervals for Figure 3 (left) and Figure 3 (middle and right).

When atmospheric initial and ice strength perturbations are combined like in STOINI, the spread generated by the individual configurations adds up resulting in larger spread for STOINI compared to INI 5 days into the forecast (Figure 2, fourth row). This accumulative effect is considerable for days 1 to 10 and reduces for longer lead time (Figure 3); spread of STOINI and INI become basically indistinguishable for most areas after about 1 month for winter start dates (Figure 3, right) and 3 weeks for summer start dates (not shown). Only along the coastlines does the stochastic parametrization lead to increased spread beyond the first month of the forecast. This might at least partly be explained by increased (reduced) mean thicknesses in the western (eastern) Arctic caused by the stochastic perturbations [see *Juricke and Jung*, 2014]. The ensemble spread of FULLINI stays significantly above the levels of the other three configurations during the first weeks almost everywhere (not shown), suggesting once more that considerable Arctic sea ice predictability originates from the atmospheric initial conditions.

3.2. Antarctic

So far, sea ice predictability studies have focused on the Arctic. Consequently, relatively little is known about Antarctic sea ice predictability (see *Holland et al.* [2013] for potential predictability estimates of Antarctic sea ice extent and the ice edge). Figure 4 (left) shows the evolution of ensemble spread for predictions of integrated Antarctic sea ice volume for all experiments. As for the Arctic, it is found that ensemble spread of Antarctic sea ice volume stays below the level of interannual variability for the entire 12 months

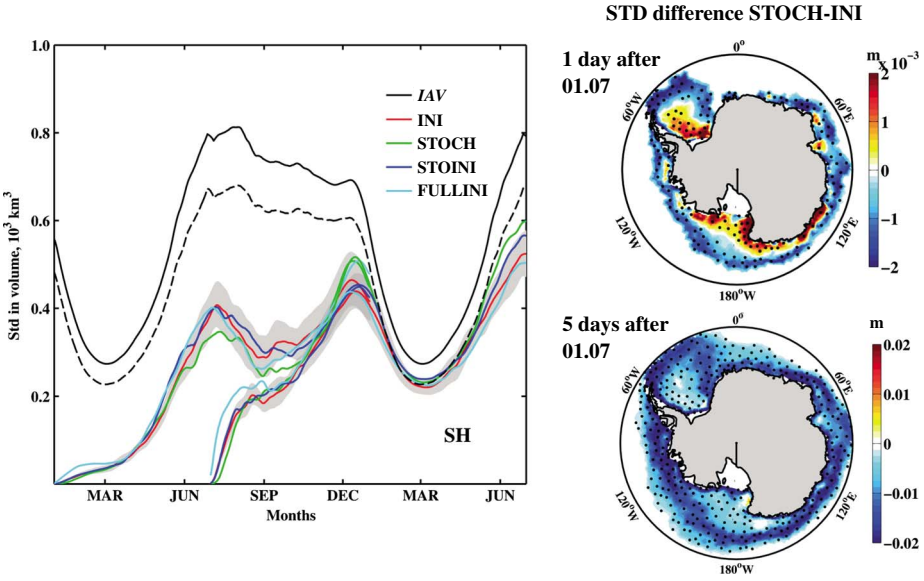

Figure 4. (left) As in Figure 1 but for the entire Antarctic sea ice volume. (right) As in Figure 2 but for the Antarctic sea ice and the difference between STOCH and INI, 1 day (top) and 5 days (bottom) after the initialization at 00 UTC on 1 July. Note the different contour intervals.

forecast period. Confidence intervals of ensemble spread and interannual variability begin to overlap after ≈11 (≈5) months into the forecasts when initialized in January (July). This implies that predictability is lost more rapidly during late growth to early melt season (July–December) compared to the late melt to early growth season (January–June) and suggests that potential predictability for Antarctic sea ice volume ranges from 5 to 11 months, depending on the start date of the forecast. Results are almost identical for Antarctic sea ice area (not shown), which is reasonable given that Antarctic sea ice volume and area are strongly correlated due to the virtual absence of thick multiyear ice. Furthermore, these findings are comparable to the results of *Holland et al.* [2013], who concluded that Antarctic sea ice extent predictability is lost during summer, but reemerges to a certain degree during the following growth season, presumably related to the rise of "ocean heat anomalies that are retained at depth over summer" [*Holland et al.*, 2013].

In the Antarctic the spread in sea ice volume generated by the different ensemble configurations becomes statistically indistinguishable earlier on in the forecast than in the Arctic. Regional distributions of the growth of Antarctic sea ice spread for the four ensemble configurations reveal large differences compared to the Arctic (Figure 4, right). Only during the first day of the forecast does STOCH produce slightly (but significantly) larger sea ice thickness spread near coastlines compared to INI (Figure 4, right (top)). By day 5, however, the atmospherically induced sea ice spread in INI outweighs the spread generated by the stochastic sea ice parameterization in STOCH almost everywhere (Figure 4, right (bottom)). This is consistent with the fact that spread levels for STOINI and INI converge toward each other within a few days into the forecast (not shown). Antarctic sea ice is comparatively thin and exhibits little dynamically formed thick multiyear ice, which results in a relatively larger impact of atmospheric initial relative to dynamical sea ice uncertainty when compared to the Arctic.

4. Discussion

The potential predictability of sea ice has been investigated using different atmospheric initial perturbation techniques and by relaxing the "perfect model" assumption through the use of a stochastic sea ice strength parameterization. Similar to previous studies it is found that sea ice exhibits considerable potential predictability on seasonal time scales, both for the Arctic and the Antarctic. From the ensemble experiments of this study it can be concluded that the potential predictability of sea ice on monthly to seasonal time scales depends only weakly on the details of how atmospheric initial uncertainty is represented; in this relatively long forecast range, adding stochastic sea ice perturbations also has a minor influence on ensemble spread and hence potential predictability estimates.

On daily to weekly time scales, however, incorporating stochastic sea ice strength perturbations in coupled model forecasts plays a surprisingly large and unique (compared to atmospheric initial perturbations) role in generating ensemble spread of sea ice thickness, especially for the Arctic. While at short lead time initial atmospheric perturbations tend to produce large spread for sea ice thickness near the ice edge, with the induced spread gradually propagating toward the central ice pack, stochastic ice strength perturbations act primarily on deformed ice under convergent motion in the central Arctic, north of Greenland and in the CAA. Differences in ensemble spread of sea ice thickness relatively early on in the forecast may have important implications, given that polar prediction is an area of growing relevance and given that proper representation of initial and model uncertainty is crucial when it comes to developing advanced ensemble and data assimilation systems. Impacts of the stochastic sea ice strength perturbations on ensemble spread of Arctic sea ice area on the other hand are small and mostly negligible throughout the entire forecast.

In the Antarctic, the impact of stochastic sea ice strength perturbations on short-term ensemble forecasts is less pronounced compared to the Arctic. This can be explained by the fact that multiyear ice is much less abundant in the Antarctic. In summary, therefore, including stochastic sea ice strength perturbations to account for model uncertainty is of greater relevance for the Arctic compared to the Antarctic.

In the future, employing a more complete set of uncertainty representations in the sea ice model, for example in the albedo parameterization, might lead to different impacts on potential predictability estimates. Recent results by *Day et al.* [2014], consistent with our findings, suggest that a more systematical investigation of the dependence of predictability on the initialization month is also desirable.

Acknowledgments
This study was supported by the TORUS-MiKlip project. Computational resources were made available by project ba0771 of the German Climate Computing Center (DKRZ) through support from the German Federal Ministry of Education and Research (BMBF), and by project hbk00032 of the North-German Supercomputing Alliance (HLRN). The authors thank Virginie Guemas and an anonymous reviewer for their helpful comments.

The Editor thanks Virginie Guemas and an anonymous reviewer for their assistance in evaluating this paper.

References

Blanchard-Wrigglesworth, E., C. M. Bitz, and M. M. Holland (2011), Influence of initial conditions and climate forcing on predicting Arctic sea ice, *Geophys. Res. Lett.*, *38*, L18503, doi:10.1029/2011GL048807.

Brankart, J.-M. (2013), Impact of uncertainties in the horizontal density gradient upon low resolution global ocean modelling, *Ocean Model.*, *66*, 64–76, doi:10.1016/j.ocemod.2013.02.004.

Bright, D. R., and S. L. Mullen (2002), Short-range ensemble forecasts of precipitation during the Southwest Monsoon, *Weather Forecasting*, *17*, 1080–1100, doi:10.1175/1520-0434(2002)017<1080:SREFOP>2.0.CO;2.

Buizza, R., M. Miller, and T. N. Palmer (1999), Stochastic representation of model uncertainties in the ECMWF ensemble prediction system, *Q. J. R. Meteorol. Soc.*, *125*, 2887–2908, doi:10.1002/qj.49712556006.

Chevallier, M., D. S. y Mélia, A. Voldoire, M. Déqué, and G. Garric (2014), Seasonal forecasts of the pan-Arctic sea ice extent using a GCM-based seasonal prediction system, *J. Clim.*, *26*, 6092–6104, doi:10.1175/JCLI-D-12-00612.1.

Danilov, S., G. Kivman, and J. Schröter (2004), A finite-element ocean model: Principles and evaluation, *Ocean Model.*, *6*, 125–150, doi:10.1016/S1463-5003(02)00063-X.

Day, J. J., S. Tietsche, and E. Hawkins (2014), Pan-Arctic and regional sea ice predictability: Initialization month dependence, *J. Clim.*, *27*, 4371–4390, doi:10.1175/JCLI-D-13-00614.1.

Holland, M. M., D. Bailey, and S. Vavrus (2011), Inherent sea ice predictability in the rapidly changing Arctic environment of the Community Climate System Model, version 3, *Clim. Dyn.*, *36*, 1239–1253, doi:10.1007/s00382-010-0792-4.

Holland, M. M., E. Blanchard-Wrigglesworth, J. Kay, and S. Vavrus (2013), Initial-value predictability of Antarctic sea ice in the Community Climate System Model 3, *Geophys. Res. Lett.*, *40*, 2121–2124, doi:10.1002/grl.50410.

Jung, T., T. N. Palmer, and G. J. Shutts (2005), Influence of a stochastic parameterization on the frequency of occurrence of North Pacific weather regimes in the ECMWF model, *Geophys. Res. Lett.*, *32*, L23811, doi:10.1029/2005GL024248.

Juricke, S., and T. Jung (2014), Influence of stochastic sea ice parameterization on climate and the role of atmosphere-sea ice-ocean interaction, *Philos. Trans. R. Soc. A*, *372*(2018), 20,130,283, doi:10.1098/rsta.2013.0283.

Juricke, S., P. Lemke, R. Timmermann, and T. Rackow (2013), Effects of stochastic ice strength perturbation on Arctic finite element sea ice modeling, *J. Clim.*, *26*, 3785–3802, doi:10.1175/JCLI-D-12-00388.1.

Koenigk, T., and U. Mikolajewicz (2009), Seasonal to interannual climate predictability in mid and high northern latitudes in a global coupled model, *Clim. Dyn.*, *32*, 783–798, doi:10.1007/s00382-008-0419-1.

Li, X., M. Charron, L. Spacek, and C. Guillem (2008), A regional ensemble prediction system based on moist targeted singular vectors and stochastic parameter perturbations, *Mon. Weather Rev.*, *136*, 443–462, doi:10.1175/2007MWR2109.1.

Lin, J. W.-B., and J. D. Neelin (2002), Considerations for stochastic convective parameterization, *J. Atmos. Sci.*, *59*, 959–975, doi:10.1175/1520-0469(2002)059<0959:CFSCP>2.0.CO;2.

Lorenz, E. N. (1963), Deterministic nonperiodic flow, *J. Atmos. Sci.*, *20*, 130–141, doi:10.1175/1520-0469(1963)020<0130:DNF>2.0.CO;2.

Lott, F., L. Guez, and P. Maury (2012), A stochastic parameterization of non-orographic gravity waves: Formalism and impact on the equatorial stratosphere, *Geophys. Res. Lett.*, *39*, L06807, doi:10.1029/2012GL051001.

Magnusson, L., J. Nycander, and E. Källén (2009), Flow-dependent versus flow-independent initial perturbations for ensemble prediction, *Tellus A*, *61*, 194–209, doi:10.1111/j.1600-0870.2008.00385.x.

Palmer, T. N. (2012), Towards the probabilistic Earth-system simulator: A vision for the future of climate and weather prediction, *Q. J. R. Meteorol. Soc.*, *138*, 841–861, doi:10.1002/qj.1923.

Plant, R. S., and G. C. Craig (2008), A stochastic parameterization for deep convection based on equilibrium statistics, *J. Atmos. Sci.*, *65*, 87–105, doi:10.1175/2007JAS2263.1.

Shutts, G. J. (2005), A kinetic energy backscatter algorithm for use in ensemble prediction systems, *Q. J. R. Meteorol. Soc.*, *131*, 3079–3102, doi:10.1256/qj.04.106.

Sidorenko, D., Q. Wang, S. Danilov, and J. Schröter (2011), FESOM under coordinated ocean-ice reference experiment forcing, *Ocean Dyn.*, *61*, 881–890, doi:10.1007/s10236-011-0406-7.

Sidorenko, D., et al. (2014), Towards multi-resolution global climate modeling with ECHAM6–FESOM. Part I: Model formulation and mean climate, *Clim. Dyn.*, doi:10.1007/s00382-014-2290-6.

Sigmond, M., J. Fyfe, G. M. Flato, V. V. Kharin, and W. J. Merryfield (2013), Seasonal forecast skill of Arctic sea ice area in a dynamical forecast system, *Geophys. Res. Lett.*, *40*, 529–534, doi:10.1002/grl.50129.

Stevens, B., et al. (2013), Atmospheric component of the MPI-M Earth System Model: ECHAM6, *J. Adv. Model. Earth Syst.*, *5*, 146–172, doi:10.1002/jame.20015.

Tietsche, S., J. J. Day, V. Guemas, W. J. Hurlin, S. P. E. Keeley, D. Matei, R. Msadek, M. Collins, and E. Hawkins (2014), Seasonal to interannual Arctic sea ice predictability in current global climate models, *Geophys. Res. Lett.*, *41*, 1035–1043, doi:10.1002/2013GL058755.

Timmermann, R., S. Danilov, J. Schröter, C. Böning, D. Sidorenko, and K. Rollenhagen (2009), Ocean circulation and sea ice distribution in a finite element global sea ice-ocean model, *Ocean Model.*, *27*, 114–129, doi:10.1016/j.ocemod.2008.10.009.

Valcke, B. (2013), The OASIS3 coupler: A European climate modelling community software, *Geosci. Model Dev.*, *6*, 373–388, doi:10.5194/gmdd-5-2139-2012.

Wang, Q., S. Danilov, and J. Schröter (2008), Finite element ocean circulation model based on triangular prismatic elements, with application in studying the effect of topography representation, *J. Geophys. Res.*, *113*, C05015, doi:10.1029/2007JC004482.

Wang, Q., S. Danilov, D. Sidorenko, R. Timmermann, C. Wekerle, X. Wang, T. Jung, and J. Schröter (2013), The Finite Element Sea ice-Ocean Model (FESOM): Formulation of an unstructured-mesh ocean general circulation model, *Geosci. Model Dev. Discuss.*, *6*, 3893–3976, doi:10.5194/gmdd-6-3893-2013.

Weisheimer, A., T. N. Palmer, and F. J. Doblas-Reyes (2011), Assessment of representations of model uncertainty in monthly and seasonal forecast ensembles, *Geophys. Res. Lett.*, *38*, L16703, doi:10.1029/2011GL048123.

Williams, P. D. (2012), Climatic impacts of stochastic fluctuations in air-sea fluxes, *Geophys. Res. Lett.*, *39*, L10705, doi:10.1029/2012GL051813.